Electronic Supplementary Material (ESI) for Journal of Materials Chemistry C.

Supporting Information

3D Topological Dirac Semimetal/MoO_3 Thin Film Heterojunction Infrared Photodetector with Current Reversal Phenomenon

Ming Yang[1], Yunkun Yang[2], Qi Liu[1], Hongxi Zhou[1], Jiayue Han[1], Xiaoyi Xie[2], Faxian Xiu[2,*], Jun Gou[1,3], Zhiming Wu[1,3], Zehua Hu[4], Ting Yu[4], Jun Wang[1,3,*] and Yadong Jiang[1,3]

M. Yang, Q. Liu, H. Zhou, J. Han

[1]School of Optoelectronic Science and Engineering, University of Electronic Science and Technology of China
Chengdu 610054, P.R. China

Y. Yang, X. Xie, Prof. F. Xiu

[2]State Key Laboratory of Surface Physics and Department of Physics, Fudan University, Shanghai 200433, P.R. China.
E-mail: faxian@fudan.edu.cn

Prof. G. Jun, Prof. Z. Wu, Prof. J. Wang, Prof. Y. Jiang

[1]School of Optoelectronic Science and Engineering, University of Electronic Science and Technology of China
Chengdu 610054, P.R. China
[3]State Key Laboratory of Electronic Thin Films and Integrated Devices, University of Electronic Science and Technology of China
Chengdu 610054, P.R. China
E-mail: wjun@uestc.edu.cn

Z. Hu, Prof. T. Yu

[4]Division of Physics and Applied Physics, School of Physical and Mathematical Sciences, Nanyang Technological University
Singapore 637371, Singapore

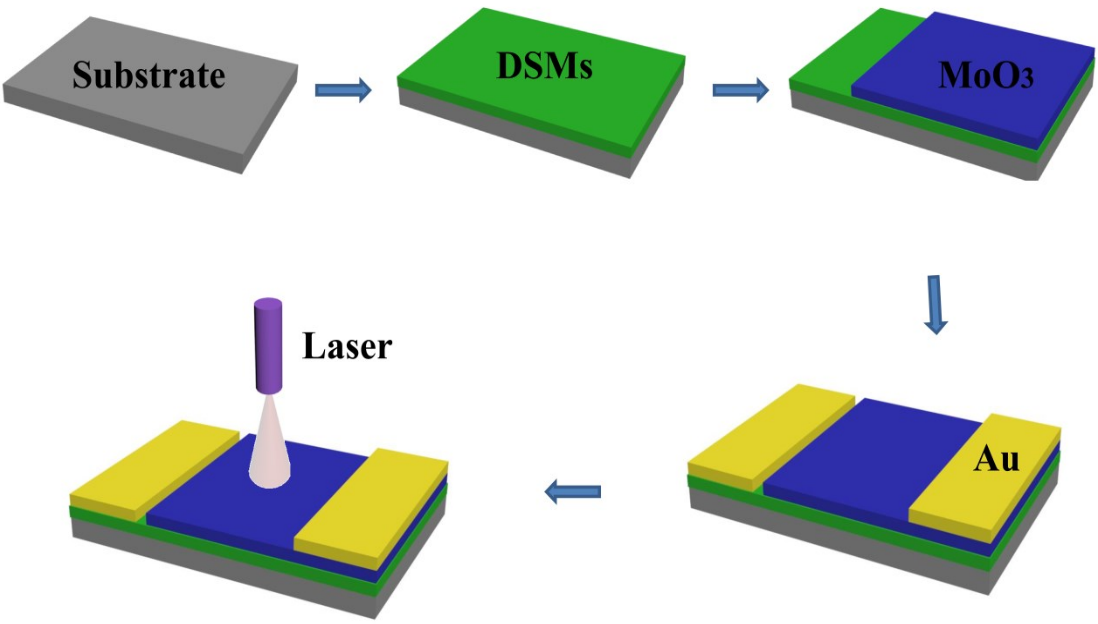

Fig. S1 Schematic diagram of the fabrication process of DSMs thin film/MoO_3 composite thin film and array device.

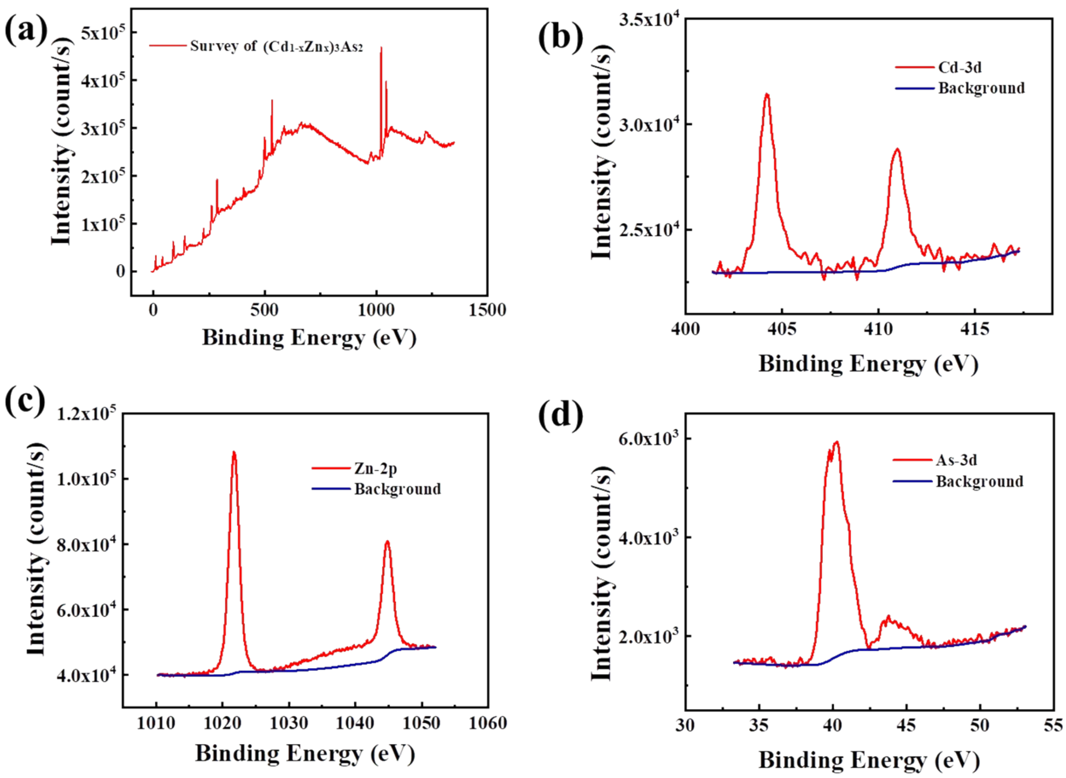

Fig. S2 XPS pattern of 100 nm $Cd_{1-x}Znx)_3As_2$ thin film. (a) The XPS survey curve of $Cd_{1-x}Znx)_3As_2$ thin film. (b),(c),(d) The XPS peak curve of Cd, Zn, As element.

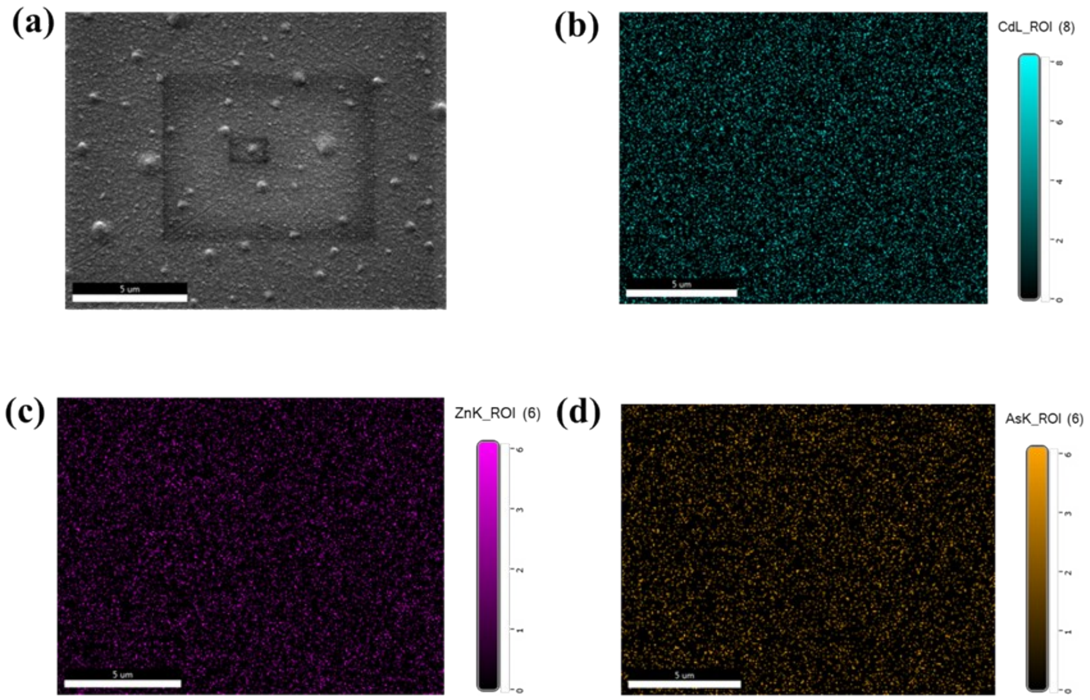

Fig. S3 EDS mapping of $(Cd_{1-x}Znx)_3As_2$ thin films. (a) Image of test area. (b), (c), (d) The EDS mapping images of Cd, Zn and As element, respectively.

Table S1 The charge transport properties (mobility, carrier type and conductivity) of prepared $(Cd_{1-x}Zn_x)_3As_2$ thin film.

Sample	**$(Cd_{1-x}Znx)_3As_2$ thin film (100 nm)**		
Carrier type	**N**	**Hall coefficient (cm^3/C)**	**-26.8**
Carrier surface density (cm^{-2})	**2.3E12**	**Resistivity (Ωcm)**	**1.6**
Carrier body density (cm^{-3})	**2.3E17**	**Conductivity (1/Ωcm)**	**0.6**
Carrier mobility (cm^2/Vs)	**16.3**	**f factor**	**0.99**

Note:Test method: Vanderbilt method

The calculation formula is as follows:

$n=B/(eR_{xy}t)$, where e is the element charge and t is the thickness of the sample.

$\mu=2206*R_{xy}/B/R_{xx}$ (unit: cm^2 / Vs)

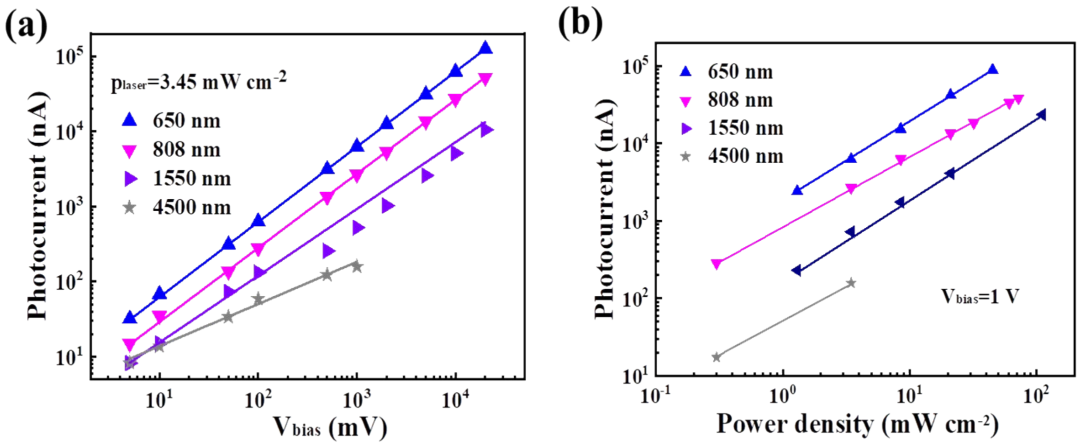

Fig. S4 (a) The I_{ph} curves of device as a function under different V_{bias}. (b) The I_{ph} curves of device as a function under different power density, while V_{bias}=1 V.

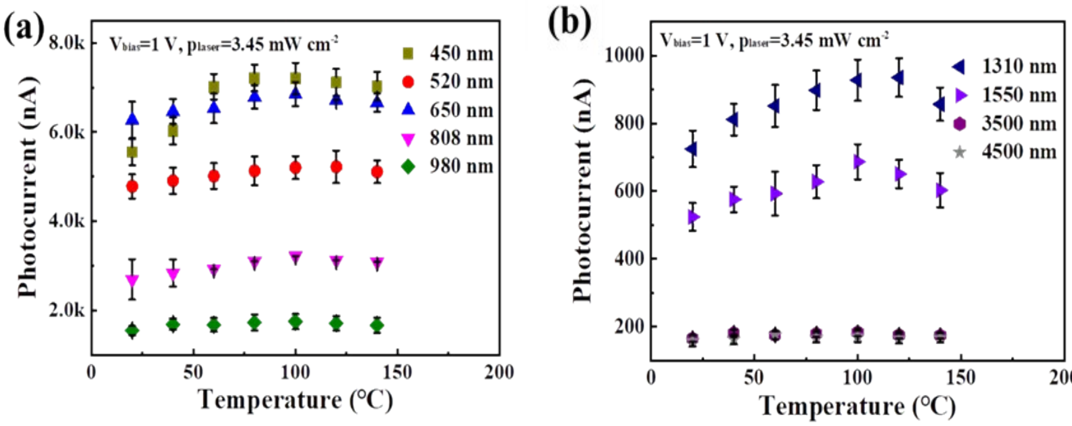

Fig. S**5** (a), (b) The performance influence of different annealing temperatures (20 °C, 40 °C, 60 °C, 80 °C, 100 °C, 120 °C, 140 °C) on $(Cd_{1-x}Zn_x)_3As_2/MoO_3$ thin film heterojunction device.

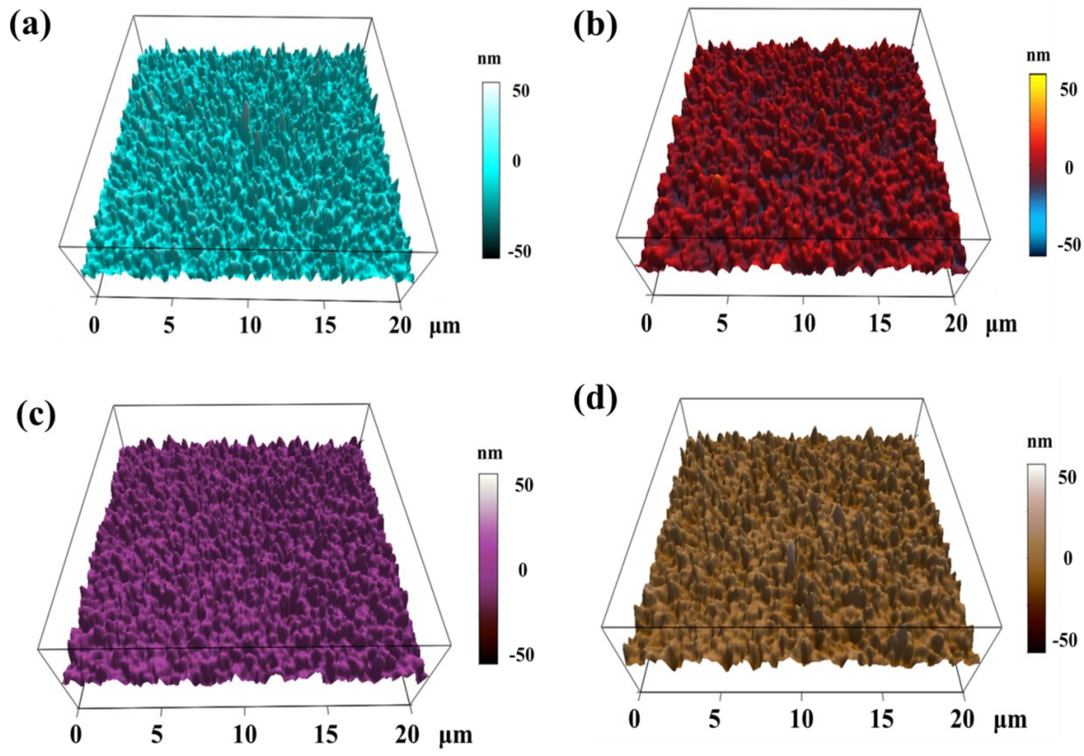

Fig. S6 (a), (b), (c), (d) The surface topography of $(Cd_{1-x}Zn_x)_3As_2$ thin film at different temperatures (20 ºC, 80 ºC, 100 ºC, 140 ºC). The test area was 20 μm×20 μm. The RMS roughness of $(Cd_{1-x}Zn_x)_3As_2$ thin film under different post-growth anneal temperatures is 22.2 nm, 19.3 nm, 17.0 nm, 18.8 nm, respectively.

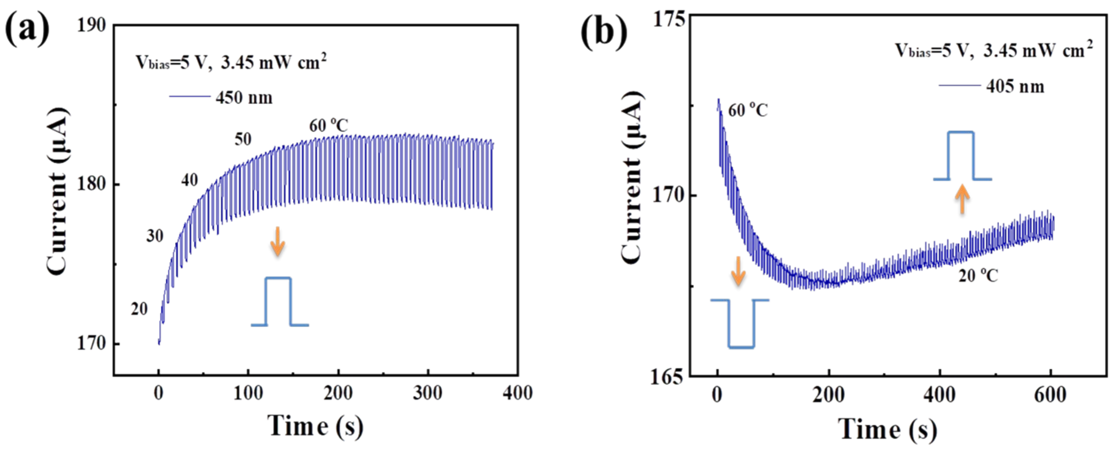

Fig. S7 Current variation characterization of $(Cd_{1-x}Zn_x)_3As_2/MoO_3$ (50 nm/100 nm) device. (a), (b) The heating and cooling process of $(Cd_{1-x}Zn_x)_3As_2/MoO_3$ (50 nm/100 nm) device, respectively.

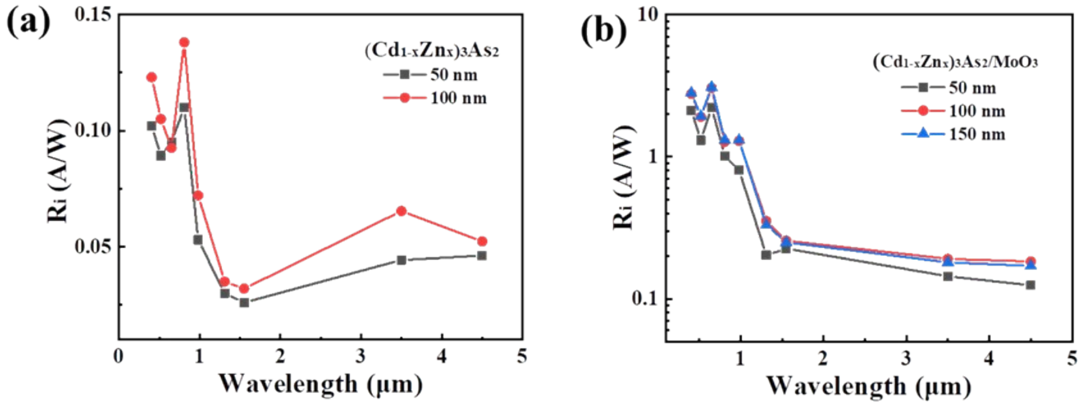

Fig. S8 (a) The R_i curves of different thickness $(Cd_{1-x}Zn_x)_3As_2$ thin film photodetectors at different wavebands. **(b)** The R_i curves of 100 nm $(Cd_{1-x}Zn_x)_3As_2$ with different thickness of MoO_3 at different wavebands.

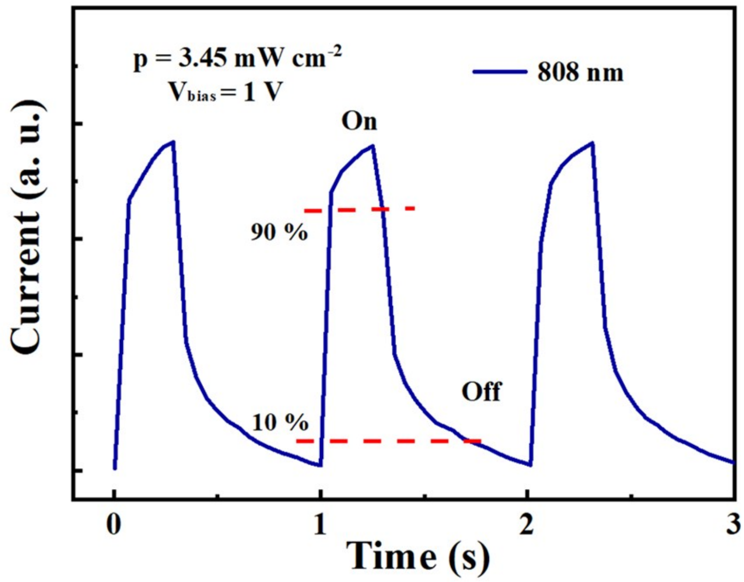

Fig. S9 The response time of $(Cd_{1-x}Zn_x)_3As_2/MoO_3$ heterojunction thin film photodetector @ 808 nm. The rise time (τ_{on}) and decay time (τ_{off}) are obtained by defining the time for the photocurrent rising from 10 % to 90 % and declining from 90 % to 10 %, respectively

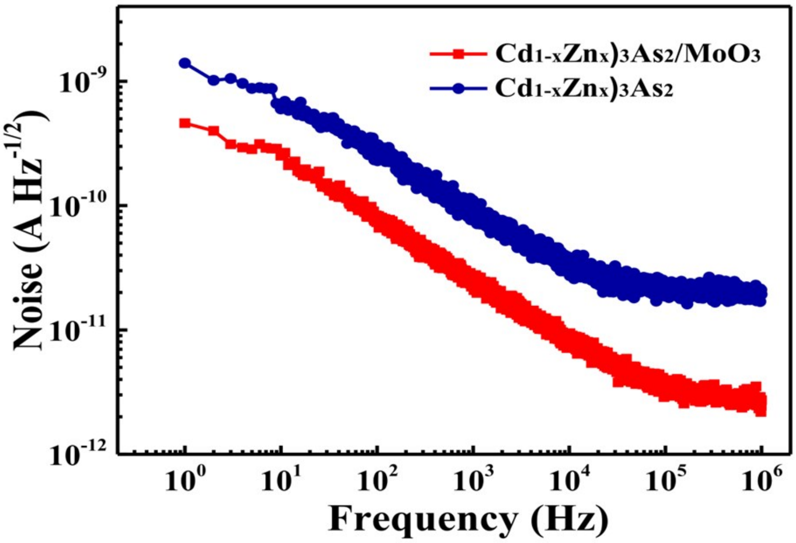

Fig. S10 The noise diagram of pure DSMs thin film device and DSMs/MoO_3 thin film heterojunction device.

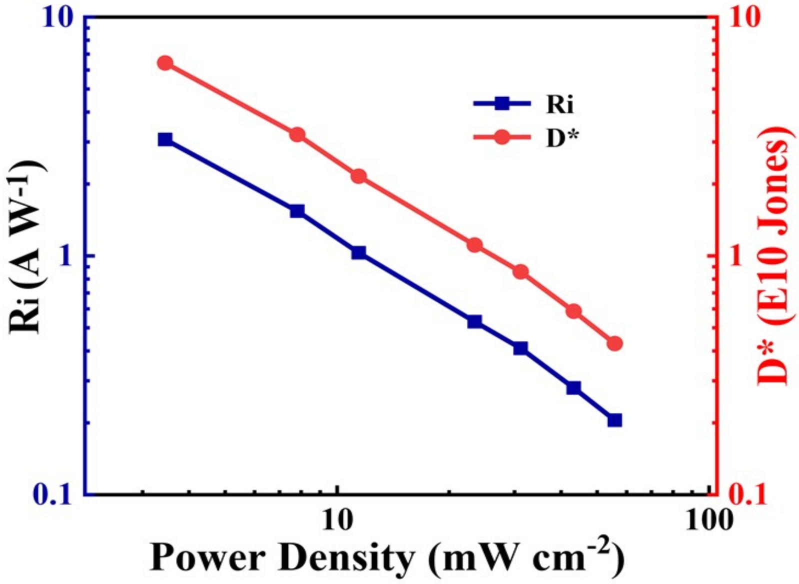

Fig. S11 The relationship between the R_i and $D*$ of the DSMs/MoO_3 thin film heterojunction device and the laser power density changes. With the decrease of the laser power, the R_i and $D*$ increase linearly.

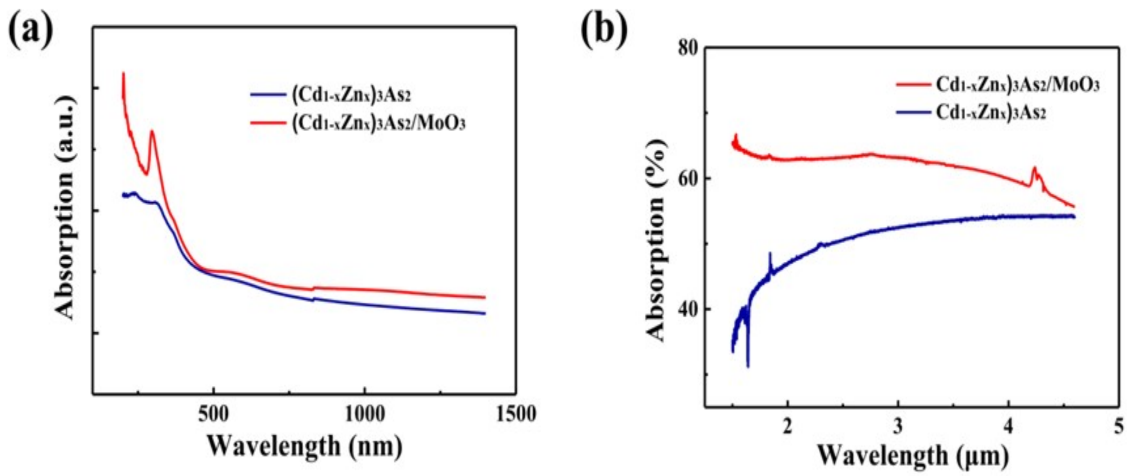

Fig. S12 The absorption curves of $(Cd_{1-x}Zn_x)_3As_2/MoO_3$ combined thin films from VL to MLIR region. (a) The region from 200 nm to 1400 nm. (b) The region from 1.5 μm to 4.6 μm.